Chemical Science

ROYAL SOCIETY OF CHEMISTRY

EDGE ARTICLE

View Article Online
View Journal | View Issue

Cite this: *Chem. Sci.*, 2025, **16**, 10333

All publication charges for this article have been paid for by the Royal Society of Chemistry

Received 27th March 2025
Accepted 29th April 2025

DOI: 10.1039/d5sc02349a

rsc.li/chemical-science

Brush-modified fluorescent organic nanoparticles by ATRP with rigidity-regulated emission†

Rongguan Yin, [a] Lianshun Luo, [a] Xiaolei Hu, [a] Hironobu Murata,[a] Jaepil Jeong, [a] Feng Gao,[b] Zijie Qiu, *[b] Ben Zhong Tang,[bc] Michael R. Bockstaller *[d] and Krzysztof Matyjaszewski *[a]

Organic nanoparticles provide exceptional intraparticle tailorability, enabling the incorporation of functional molecules for diverse applications. In this study, we present the synthesis and characterization of fluorescent organic nanoparticles (FoNPs) with encapsulated aggregation-induced emission (AIE) luminogens with emission properties regulated by particle rigidity. Atom transfer radical polymerization (ATRP) was employed in dispersed media to develop various fluorescence colors tuned by precise control over particle rigidity. Comprehensive analyses revealed that increased particle rigidity significantly enhanced photoluminescence, achieving quantum yields of up to 22% in selected solvents. The high chain-end fidelity facilitated the grafting of hydrophilic polymer brushes from surfaces of FoNPs used as macroinitiators, enabling their dispersion in aqueous media while maintaining bright fluorescence. These findings highlight the potential of rigidity-regulated FoNPs as versatile platforms for advanced material applications, particularly in fluorescent waterborne films and aqueous-phase sensing systems.

Introduction

Brush-modified nanoparticles are precisely designed nanomaterials in which polymer chains are tethered to nanoparticle cores.[1–5] Their properties are highly customizable, as the macromolecular characteristics of the brush layer can be tailored to suit the nanoscale constituents. The interactions between the components can lead to synergistic enhancement of properties, enabling these materials to meet specific application requirements.[6–10] While significant attention has been given to grafting polymers from surfaces of inorganic nanoparticles, organic nanoparticles (oNPs) offer additional intraparticle tailorability.[11–13] Various functional molecules can be loaded into oNPs, while maintaining environmental compatibility and biological safety.[14] An example is the recently developed polyinimer-based oNPs,[15] which feature tunable rigidity and preserved end-group functionality, achieved through atom transfer radical polymerization (ATRP).[16–18]

Aggregation-induced emission (AIE) refers to the phenomenon where molecules exhibit enhanced emission in the aggregated form or with restricted molecular motion.[19–21] With a wide variety of AIE luminogens (AIEgens) and diverse strategies to suppress molecular motion, AIE has found extensive potential applications in lighting, imaging, and sensing.[22] AIEgen can be selectively incorporated into synthetic polymer materials[23–25] as initiators,[26] monomers,[27–29] or crosslinkers,[30] and can also endow tunable emission dependent on through-space charge transfer.[31–34] When AIEgen-based crosslinkers are incorporated into polymer networks, the matrices can sustain enhanced luminescence even in solution.[35] Despite profound research on "covalent" attachment of AIEgens in polymers, investigations into non-covalent, physically entrapped AIEgens influenced by tunable rigidity are very rare.

Herein, we developed fluorescent organic nanoparticles (FoNPs) with AIEgens physically entrapped with rigidity-regulated AIE properties using microemulsion ATRP (Fig. 1). The AIEgens were premixed with the comonomers of inimer (2-(2-bromoisobutyryloxy)ethyl methacrylate, BiBEM) and crosslinker (ethylene glycol dimethacrylate, EGDMA) reported in a previous study.[15] This mixture, prepared without organic solvents, was sonicated to form the oil phase. Two hydroxy-functionalized AIEgens, named HMTPE and THBPE (Fig. 1 and S1†), were selected due to their compatibility with BiBEM. The AIEgen loading was 3 and 0.3 mol% for smaller HMTPE and for larger THBPE, respectively. The loadings of THBPE were

[a]*Department of Chemistry, Carnegie Mellon University, Pittsburgh, Pennsylvania 15213, USA. E-mail: km3b@andrew.cmu.edu*

[b]*School of Science and Engineering, Shenzhen Institute of Aggregate Science and Technology, The Chinese University of Hong Kong, (CUHK-Shenzhen), Shenzhen, Guangdong 518172, P. R. China. E-mail: zijieqiu@cuhk.edu.cn*

[c]*Department of Chemistry, The Hong Kong Branch of Chinese National Engineering Research Center for Tissue Restoration and Reconstruction, The Hong Kong University of Science and Technology, Kowloon, Hong Kong 230026, P. R. China*

[d]*Department of Materials Science and Engineering, Carnegie Mellon University, Pittsburgh, Pennsylvania 15213, USA. E-mail: bockstal@andrew.cmu.edu*

† Electronic supplementary information (ESI) available. See DOI: https://doi.org/10.1039/d5sc02349a

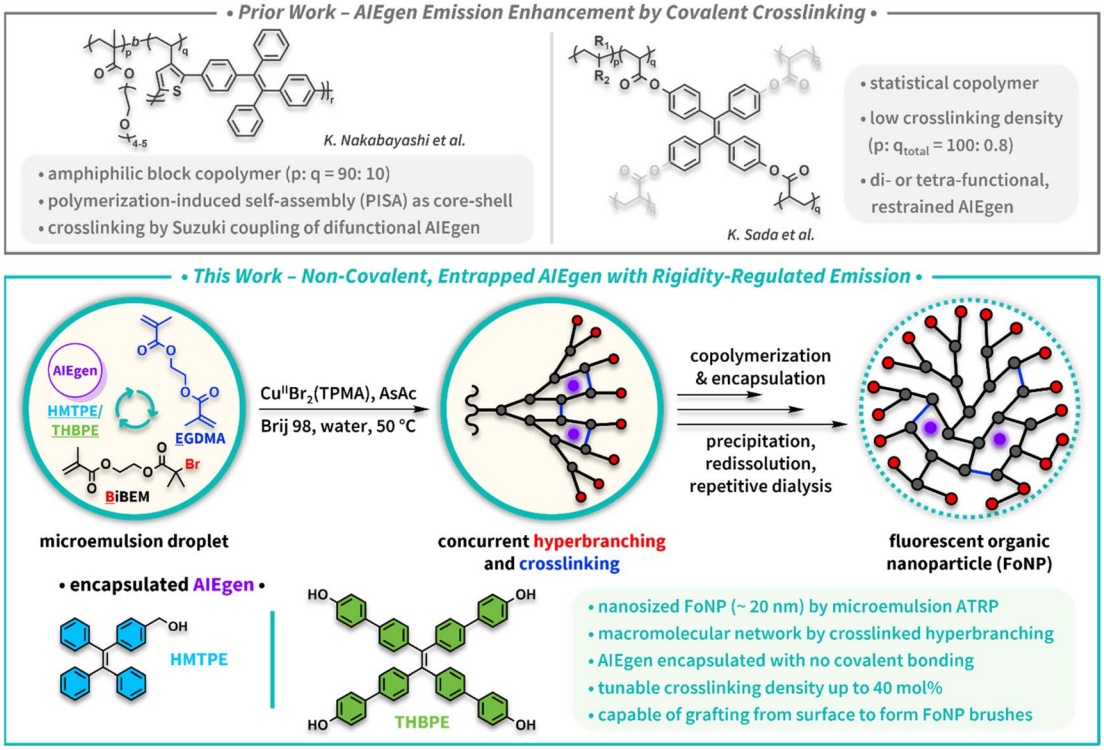

Fig. 1 Schematic illustration of AIEgen-encapsulated FoNP by microemulsion ATRP.

limited by its poorer solubility in the inimer. The non-ionic surfactant Brij 98 stabilized the oil–water interface, ensuring that each FoNP macromolecule was confined within a single microemulsion droplet.[36] The aqueous phase contained the surfactant and the copper catalyst complex [Br–Cu^{II}(TPMA)]$^+$ [TPMA = tris(2-pyridylmethyl)amine]. The oil–water mixture was homogenized through vortex mixing to form a microemulsion, followed by the addition of ascorbic acid (AsAc) as a reducing agent to initiate the ATRP reaction. The resulting FoNPs with physically trapped AIEgens were purified through precipitation in methanol, dissolution in tetrahydrofuran (THF), and repeated dialysis to remove residual unreacted reagents, leached AIEgens, and any other impurities.

Results and discussion

The purified FoNPs were designated as AIEgen$_m$BnE(100–n) (B and E represent BiBEM and EGDMA, respectively), indicating the molar fraction of each component. Three representative compositions—B90E10, B75E25, and B60E40—were selected to study the effect of increasing intraparticle rigidity. The investigation of "size change" of oNPs in microemulsion (immediately after polymerization) and redispersed states (in THF) showed a transition from "swollen" to "shrunk" states, and their enhanced intraparticle rigidity was governed by increasing crosslinker content using Brillouin light spectroscopy, as reported previously.[15] The morphology of oNPs by atomic force microscopy (AFM) and their glass transition by differential scanning calorimetry (DSC) were also reported. The FoNPs in THF solutions were characterized using size exclusion chromatography (SEC) and dynamic light scattering (DLS) to assess molecular weight and hydrodynamic size (Fig. 2a). Regardless of the type of incorporated AIEgen, DLS showed that the hydrodynamic size of the FoNP decreased with increased crosslinker content (Fig. S2†). Additionally, SEC analysis with a refractive index (RI) detector (Fig. S3†) revealed that more rigid FoNPs exhibited smaller elution volume and lower dispersity (*i.e.*, the value of M_w/M_n), consistent with reduced swelling regulated by crosslinker content. From all the characterization results using SEC and DLS, no bimodal distribution was observed, which indicated that the FoNP systems are unimolecular. Absolute molecular weights were measured using a multi-angle light scattering (MALS) detector with sample concentration adjustments. Each batch displayed molecular weights in the range of several million, indicating its compact structure. Furthermore, the similar molecular weight values across batches underscored the reproducibility of the microemulsion method, where essentially all vinyl comonomers were effectively transformed into a single crosslinked macromolecule within the confined compartments.

Spectrofluorometry was employed to investigate the photoluminescence properties of the FoNPs. The photoluminescence quantum yields (QY, Φ) were determined by measuring the absolute QY of a reference sample (Fig. S4†), and then the relative QY was calculated for other samples (eqn (S1) and Table S1†).[37] Control experiments showed that bare oNPs (without

(a) Rigidity-Regulated Emission

Entry[a]	x_{BiBEM}	x_{EGDMA}	x_{AIEgen}	$M_{n,RI}$ ($\times 10^3$)[b]	M_w/M_n[b]	$M_{n,MALS}$ ($\times 10^3$)[c]	$D_{FoNP,THF}$ (nm)[d]
$HMTPE_3B90E10$	0.90	0.10	0.03	103	1.46	3183	27.2 ± 0.5
$HMTPE_3B75E25$	0.75	0.25	0.03	57	1.25	3218	19.9 ± 0.4
$HMTPE_3B60E40$	0.60	0.40	0.03	41	1.19	3244	16.4 ± 0.3
$THBPE_{0.3}B90E10$	0.90	0.10	0.003	106	1.35	3261	25.8 ± 0.1
$THBPE_{0.3}B75E25$	0.75	0.25	0.003	61	1.24	3470	19.5 ± 0.1
$THBPE_{0.3}B60E40$	0.60	0.40	0.003	46	1.20	4252	18.0 ± 0.2

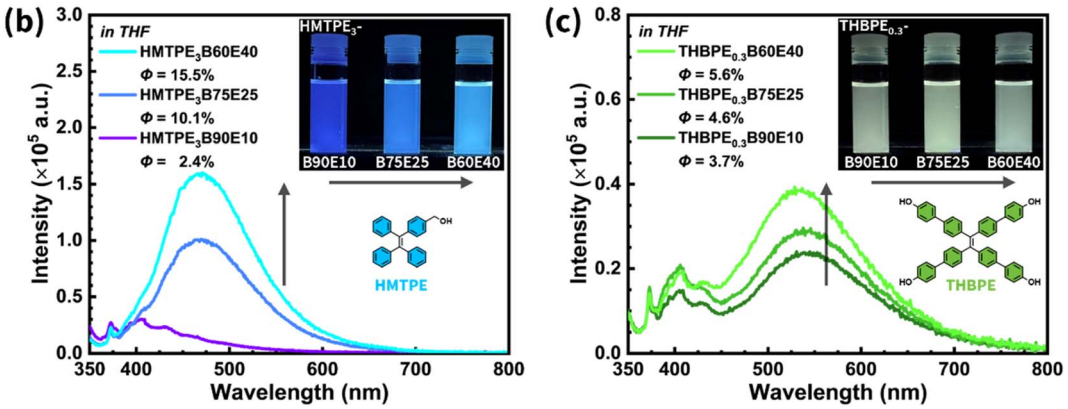

Fig. 2 AIEgen-encapsulated FoNP with rigidity-regulated emission. (a) Sample information. [a]Reaction conditions: $[AIEgen]_0$: $[BiBEM]_0$: $[EGDMA]_0$: $[CuBr_2(TPMA)]_0$: $[AsAc]_0 = 3$ (HMTPE) or 0.3 (THBPE): n: 100−n: 0.08: 0.4, BiBEM 0.5 × (n/100) g, Brij 98 0.5 g in 12 g water, 50 °C for 2 h. [b]Apparent molecular weights (and distributions) of FoNPs determined by THF SEC using RI detector and PMMA standards. [c]Absolute molecular weights determined by MALS detector and calibrated using sample mass concentration. [d]Hydrodynamic diameters determined by DLS based on the volume distribution in THF. Fluorescent emission spectra evolution (excitation wavelength $\lambda_{ex} = 336$ nm) of (b) HMTPE- and (c) THBPE-encapsulated FoNPs with increasing intraparticle rigidity (served by the arrow to guide the eye). (Inset) Digital photos of FoNPs under UV irradiation ($\lambda_{ex} = 365$ nm).

AIEgens) exhibited weak fluorescence (QYs ~3%) (Fig. S5†). This could be partially attributed to the residual copper catalyst complex entrapped during the polymerization (Fig. S6†).[38] The absorption and emission spectra of both AIEgens, in THF solutions and the solid state, were analyzed (Fig. S7†). Compared to the spectra of AIEgen-encapsulated FoNPs, although the oNP backbone influenced the absorption spectrum, the emission of FoNP (despite a slight red shift) resembled that of solid AIEgen. Based on these observations, the QYs of FoNPs were comparable.

For HMTPE-encapsulated FoNPs, a significant increase in emission intensity was observed as intraparticle rigidity increased (Fig. 2b). The most rigid $HMTPE_3B60E40$ exhibited a QY of 15.5%, as confirmed by the cyan fluorescence. In contrast, the least rigid $HMTPE_3B90E10$ showed a QY of only 2.4%, similar to that of bare oNPs. The low QY was attributed to insufficient rigidity within the FoNP, which allowed unrestricted local intramolecular motion and resulted in weak emission from HMTPE despite successful encapsulation (Fig. S8†). Further control experiments, in which particle rigidity was maintained while varying the HMTPE composition, demonstrated consistent QY values (Fig. S9†). Increasing the number of AIEgens per FoNP did not enhance emission, confirming that intraparticle rigidity, rather than potential aggregation, is a critical factor for photoluminescence enhancement.

For THBPE, which features a larger molecular scaffold, encapsulation produced FoNPs with a specific emission peak around 540 nm (Fig. 2c). A steady increase in QY was observed as FoNP rigidity increased; however, the enhancement was less pronounced, likely due to the difficulty in fully restricting the rotational motion of the larger molecules. Nonetheless, the combined emissions from the oNP backbone and THBPE generated weak greenish-white fluorescence under UV irradiation (Fig. S10†), representing a rare instance of full-spectrum emission using a single dye.[39]

The "skeletal" densities of solid oNP backbones were previously measured by a helium pycnometer to be approximately 1.43 g cm^{-3}.[15] Based on available data—including molecular weight, hydrodynamic size, and the skeletal volume of oNPs

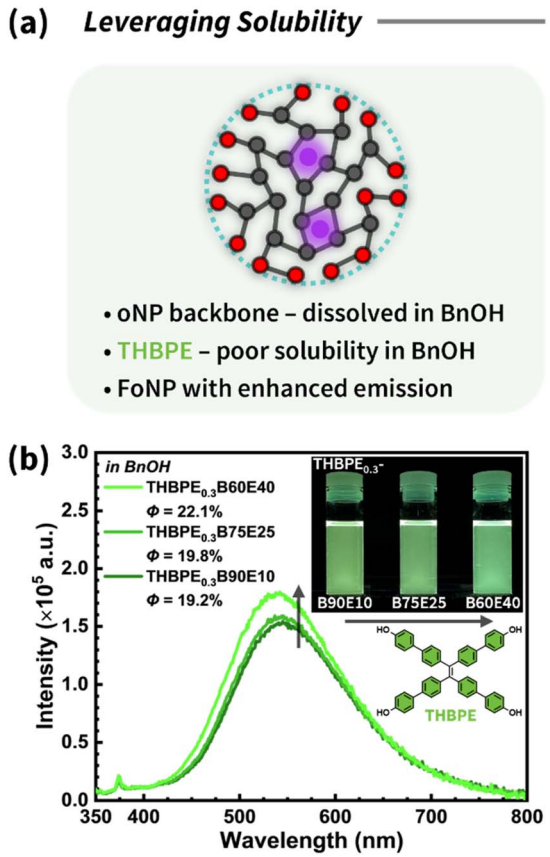

Fig. 3 THBPE-encapsulated FoNP with enhanced emission in BnOH. (a) Schematic illustration of solubility difference between oNP backbone and THBPE to generate a brighter emission. (b) Fluorescent emission spectra evolution (λ_{ex} = 336 nm) of THBPE-encapsulated FoNPs with increasing intraparticle rigidity (served by the arrow to guide the eye). (Inset) Digital photo of FoNPs under UV irradiation (λ_{ex} = 365 nm).

measured with the pycnometer—the porosities of the oNP backbones were estimated (Table S2†). They ranged from 73% for B90E10 to 32% for B60E40, suggesting that solvent molecules could penetrate FoNP. Therefore, benzyl alcohol (BnOH), a polar solvent, was selected to explore an alternative approach for enhancing emissions where the oNP backbone could fully disperse while the AIEgen remained poorly soluble (Fig. 3a). While THBPE exhibited poor solubility in BnOH, the THBPE-encapsulated FoNPs formed a clear and transparent dispersion in BnOH after ultrasonication (Fig. S11†). In these dispersions, the FoNPs exhibited bright yellow-green fluorescence, with their QY increasing to 22.1% (Fig. 3b). Notably, QY continued to increase with enhanced FoNP rigidity, further underscoring the phenomenon of rigidity-regulated emissions.

ATRP retains high chain-end fidelity in the synthesized macromolecules needed for chain extension.[40] Leveraging the high bromide content from BiBEM, the FoNPs served as macroinitiators (*i.e.*, FoNP-Br) for grafting polymer brushes directly from their surfaces. In a model reaction, ethyl α-bromoisobutyrate (EBiB) was used as a sacrificial initiator to estimate the molecular weight of the grafted chains (Fig. 4a).[41] Hydrophilic oligo(ethylene glycol) methyl ether methacrylate ($OEOMA_{500}$, average M_n = 500) was selected as the monomer for the brush layer to effectively disperse the entire particle brush in water while the contracted FoNP core contributed to enhanced emission (Fig. 4b). This approach overcame the traditional limitation of AIEgens, which typically aggregate in water to emit.

To achieve this, surface-initiated activators regenerated by electron transfer (SI-ARGET) ATRP was employed, using tin(II) 2-ethylhexanoate [$Sn(Oct)_2$] as the reducing agent. Mixtures of $POEOMA_{500}$-grafted FoNPs (FoNP-*g*-$POEOMA_{500}$) and linear $POEOMA_{500}$ were partially diluted in dimethylformamide (DMF) for SEC analysis. The analysis revealed that the elution time of FoNP-*g*-$POEOMA_{500}$ shifted toward higher molecular weights compared to the original FoNPs, confirming the preservation of end-group functionality and growth of chains from the surface of particles (Fig. 4c). The peak corresponding to linear $POEOMA_{500}$ was deconvoluted (assuming a normal distribution) and calibrated using the Mark–Houwink equation to determine its absolute molecular weight (Fig. S12, eqn (S2) and (S3)†).[42,43]

Grafting density (σ, chains nm^{-2}) is a critical parameter for nanoparticle brushes, quantifying the number of polymer chains grafted per unit surface area.[44] The comprehensive method used for the σ determination of FoNP-*g*-$POEOMA_{500}$ is outlined in the ESI (eqn (S4)–(S14) and Table S3),† and the consolidated results are shown in Fig. 4d. The effectiveness of FoNP-Br with its multiple initiating sites was demonstrated by the average number of grafted polymer chains (N_{brush}). Results showed that N_{brush} decreased as FoNP rigidity increased. Despite this reduction and the smaller hydrodynamic sizes, the σ values remained high, ranging from 0.7 to 0.9 chain per nm^2, a level for assembling ordered nanostructures.[45] Each brush-modified FoNP exhibited an average molar mass of up to 133 × 10^6 g mol^{-1}, indicating a gigantic macromolecule. The average number of AIEgens per FoNP was also estimated, reaching approximately 358 for HMTPE- and 42 for THBPE-encapsulated FoNPs, respectively. Assuming no aggregation and even distribution, these values correspond to an approximate average distance of 2.3 nm for HMTPE and 4.8 nm for THBPE between neighboring AIEgens.

To validate the concept, particle brushes were purified using ultrahigh-speed centrifugation to separate them from linear polymers. The centrifuged $HMTPE_3B60E40$-*g*-$POEOMA_{500}$ particle brushes were redispersed in water (20 mg mL^{-1}), forming a transparent dispersion (Fig. S13†). In contrast, $HMTPE_3B60E40$ (FoNP without brushes) was diluted in THF (0.8 mg mL^{-1}) to achieve an equivalent HMTPE concentration (9.2 × 10^{-5} mol L^{-1}). When irradiated with UV light, the water-dispersed particle brushes emitted significantly brighter fluorescence (Fig. 4e). These experiments demonstrate the potential for applying physically entrapped AIEgen-based materials in aqueous environments and highlight brush-modified FoNPs as promising candidates for fluorescent waterborne coating materials.

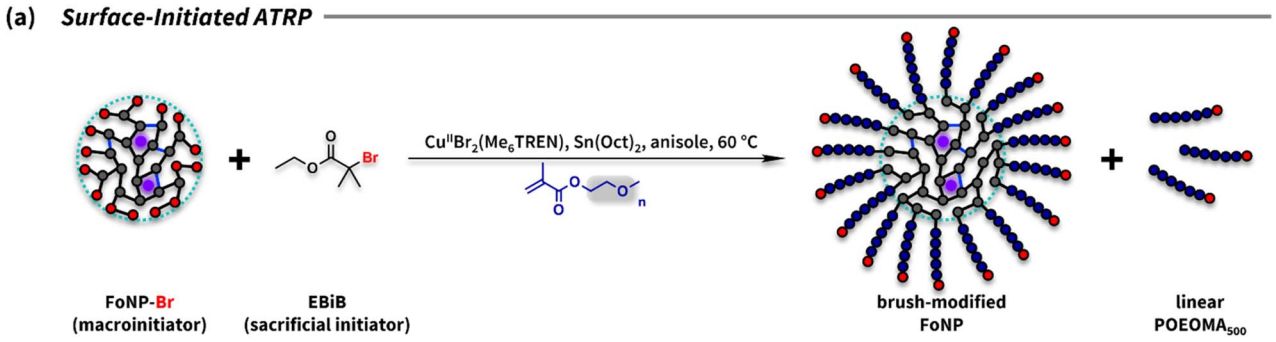

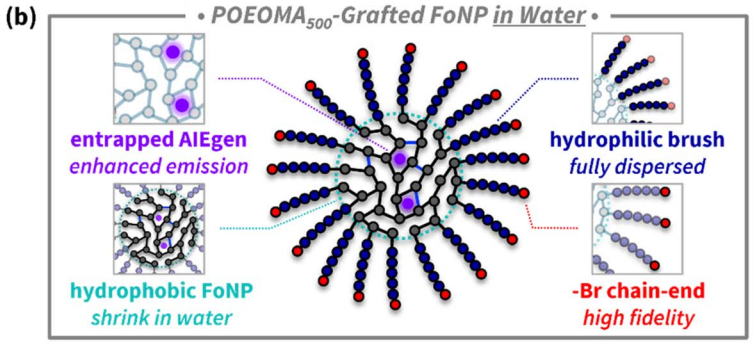

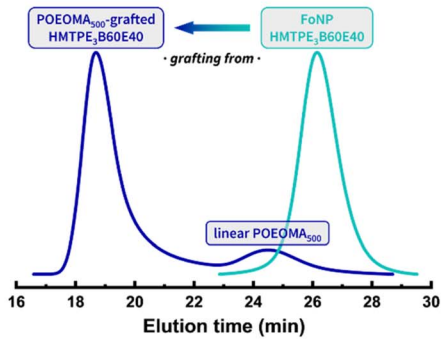

(d)

Entry[a]	$M_{n,\,brush}$[b]	M_w/M_n[b]	N_{brush}[c]	σ (nm^{-2})[c]	$M_{n,\,PGFoNP}$ (× 10^6)[c]
HMTPE$_3$B90E10SI	82000	1.21	1585	0.68	133
HMTPE$_3$B75E25SI	101700	1.38	977	0.79	103
HMTPE$_3$B60E40SI	112840	1.24	698	0.83	82
THBPE$_{0.3}$B90E10SI	73520	1.29	1627	0.78	123
THBPE$_{0.3}$B75E25SI	99700	1.35	961	0.80	99
THBPE$_{0.3}$B60E40SI	116000	1.38	886	0.87	107

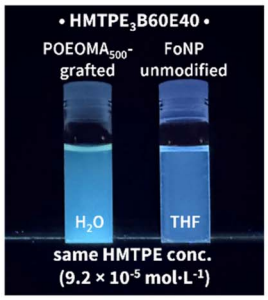

Fig. 4 SI-ARGET ATRP from FoNP-Br macroinitiator with EBiB. Schematic illustration of the (a) synthesis and (b) emission enhancement of brush-modified FoNP. (c) (Normalized) SEC elution time of HMTPE$_3$B60E40 (in THF, green) and mixtures of HMTPE$_3$B60E40-*g*-POEOMA$_{500}$ with linear POEOMA$_{500}$ (in DMF, blue). (d) Sample information. [a]Reaction conditions: the bromide concentration of macroinitiator ([FoNP-Br]$_0$) was denoted as an unknown *x*; [OEOMA$_{500}$]$_0$: [FoNP-Br]$_0$: [EBiB]$_0$: [CuBr$_2$]$_0$: [Me$_6$TREN]$_0$: [Sn(Oct)$_2$]$_0$ = 10 000: *x*: 1: 3: 9: 15, FoNP-Br approximately 50 mg, OEOMA$_{500}$ 6 mL (50 vol% in anisole), 60 °C for 1 h. [b]Absolute molecular weights and distributions of the grafted POEOMA$_{500}$ brush layer calibrated using Mark–Houwink equation. [c]Calculated average number of grafted chains per FoNP-Br, grafting density, and molecular weight of FoNP-*g*-POEOMA$_{500}$ were detailed in the ESI.† (e) Digital photo of HMTPE$_3$B60E40-*g*-POEOMA$_{500}$ (in water, 20 mg mL^{-1}) and HMTPE$_3$B60E40 (in THF, 0.8 mg mL^{-1}) with equivalent HMTPE concentration (9.2 × 10^{-5} mol L^{-1}) under UV irradiation (λ_{ex} = 365 nm).

Conclusions

In summary, this study revealed the integrated synthesis and comprehensive characterization of AIEgen-encapsulated FoNPs with rigidity-regulated emission, achieved through micro-emulsion ATRP. The modular design, allowing precise control over key FoNP properties such as AIEgen type and intraparticle rigidity, highlighted the versatility of the physical entrapment approach in developing highly customizable fluorescent nanoparticle systems. Additionally, the high chain-end fidelity enabled by ATRP facilitated the efficient surface grafting of hydrophilic polymer brushes. The investigation into the grafting density of brush-tethered FoNPs underscored their potential for uniform self-assembly into nanostructures. These brush-modified FoNPs demonstrated enhanced photoluminescence at low dye loading without covalent attachments and with full dispersibility in water, overcoming traditional limitations of AIEgens. This work broadens the scope of AIE applications in the aqueous environment and establishes brush-modified FoNPs as promising candidates for fluorescent waterborne film materials.

Data availability

ESI data† have been included in the article's ESI.† These include experimental procedures; additional absorption and photoluminescence emission spectra; quantum yield determinations; additional characterization results; detailed calculations on porosity (of oNP backbones) and grafting density (of brush-modified FoNPs).

Author contributions

R. Y., X. H., and H. M. completed the synthesis. R. Y., L. L., and J. J. performed material characterization work. F. G., Z. Q., and B. Z. T. provided support on result interpretation. M. R. B. and K. M. conceived and organized the project, and together with R. Y. wrote the manuscript.

Conflicts of interest

There are no conflicts to declare.

Acknowledgements

The authors highly appreciate the support from Prof. Rongchao Jin. This material is based upon work supported by the U.S. Department of Energy, Office of Science, Office of Basic Energy Sciences, under award number DE-SC0018784. The authors further acknowledge financial support by the National Science Foundation *via* DMR 2209587 (MB) and DMR 2202747 (KM). The authors further acknowledge the Materials Characterization Facility at Carnegie Mellon University under grant # MCF-677785.

References

1 J. O. Zoppe, N. C. Ataman, P. Mocny, J. Wang, J. Moraes and H.-A. Klok, Surface-Initiated Controlled Radical Polymerization: State-of-the-Art, Opportunities, and Challenges in Surface and Interface Engineering with Polymer Brushes, *Chem. Rev.*, 2017, **117**, 1105–1318.

2 S. K. Kumar, B. C. Benicewicz, R. A. Vaia and K. I. Winey, 50th Anniversary Perspective: Are Polymer Nanocomposites Practical for Applications?, *Macromolecules*, 2017, **50**, 714–731.

3 J. Yan, M. R. Bockstaller and K. Matyjaszewski, Brush-modified materials: Control of molecular architecture, assembly behavior, properties and applications, *Prog. Polym. Sci.*, 2020, **100**, 101180.

4 H. He, X. Shen and Z. Nie, Engineering interactions between nanoparticles using polymers, *Prog. Polym. Sci.*, 2023, **143**, 101710.

5 T. Hueckel, X. Luo, O. F. Aly and R. J. Macfarlane, Nanoparticle Brushes: Macromolecular Ligands for Materials Synthesis, *Acc. Chem. Res.*, 2023, **56**, 1931–1941.

6 N. Corrigan, X. Shi and C. Boyer, Diblock Copolymer Stabilized Liquid Metal Nanoparticles: Particle Settling Behavior and Application to 3D Printing, *ACS Macro Lett.*, 2023, **12**, 241–247.

7 R. Yin, Y. Zhao, J. Jeong, J. Tarnsangpradit, T. Liu, S. Y. An, Y. Zhai, X. Hu, M. R. Bockstaller and K. Matyjaszewski, Composition-Orientation Induced Mechanical Synergy in Nanoparticle Brushes with Grafted Gradient Copolymers, *Macromolecules*, 2023, **56**, 9626–9635.

8 Y. Zhao, H. Wu, R. Yin, C. Yu, K. Matyjaszewski and M. R. Bockstaller, Copolymer Brush Particle Hybrid Materials with "Recall-and-Repair" Capability, *Chem. Mater.*, 2023, **35**, 6990–6997.

9 G. J. Desroches, C. J. Thrasher, N. S. Diaco, I. O. Raji, D. Konkolewicz, A. J. Hart and R. J. Macfarlane, Multivalent Polymer-Grafted Nanoparticles as Reinforcing Fillers for 3D Printable Self-Healing Elastomers, *ACS Mater. Lett.*, 2024, **6**, 4175–4182.

10 Y. Zhao, Z. Wang, C. Yu, H. Wu, M. Olszewski, R. Yin, Y. Zhai, T. Liu, A. Coronado, K. Matyjaszewski and M. R. Bockstaller, Topologically Induced Heterogeneity in Gradient Copolymer Brush Particle Materials, *Macromolecules*, 2022, **55**, 8846–8856.

11 K. Margulis-Goshen and S. Magdassi, Organic nanoparticles from microemulsions: Formation and applications, *Curr. Opin. Colloid Interface Sci.*, 2012, **17**, 290–296.

12 J. Han, Y. Zhai, Z. Wang, M. Bleuel, T. Liu, R. Yin, W. Wu, I. F. Hakem, A. Karim, K. Matyjaszewski and M. R. Bockstaller, Nanosized Organo-Silica Particles with "Built-In" Surface-Initiated Atom Transfer Radical Polymerization Capability as a Platform for Brush Particle Synthesis, *ACS Macro Lett.*, 2020, **9**, 1218–1223.

13 K. K. Ng and G. Zheng, Molecular Interactions in Organic Nanoparticles for Phototheranostic Applications, *Chem. Rev.*, 2015, **115**, 11012–11042.

14 F. Fang, M. Li, J. Zhang and C.-S. Lee, Different Strategies for Organic Nanoparticle Preparation in Biomedicine, *ACS Mater. Lett.*, 2020, **2**, 531–549.

15 R. Yin, J. Tarnsangpradit, A. Gul, J. Jeong, X. Hu, Y. Zhao, H. Wu, Q. Li, G. Fytas, A. Karim, M. R. Bockstaller and K. Matyjaszewski, Organic nanoparticles with tunable size and rigidity by hyperbranching and cross-linking using microemulsion ATRP, *Proc. Natl. Acad. Sci. U. S. A.*, 2024, **121**, e2406337121.

16 K. Matyjaszewski, Advanced Materials by Atom Transfer Radical Polymerization, *Adv. Mater.*, 2018, **30**, 1706441.

17 X. Hu, R. Yin, J. Jeong and K. Matyjaszewski, Robust Miniemulsion PhotoATRP Driven by Red and Near-Infrared Light, *J. Am. Chem. Soc.*, 2024, **146**, 13417–13426.

18 S. Harrisson, R. Whitfield, A. Anastasaki and K. Matyjaszewski, Atom transfer radical polymerization, *Nat. Rev. Methods Primers*, 2025, **5**, 2.

19 Z. Zhao, H. Zhang, J. W. Y. Lam and B. Z. Tang, Aggregation-Induced Emission: New Vistas at the Aggregate Level, *Angew. Chem., Int. Ed.*, 2020, **59**, 9888–9907.

20 W.-J. Wang, Z.-Y. Xin, X. Su, L. Hao, Z. Qiu, K. Li, Y. Luo, X.-M. Cai, J. Zhang, P. Alam, J. Feng, S. Wang, Z. Zhao and B. Z. Tang, Aggregation-Induced Emission Luminogens Realizing High-Contrast Bioimaging, *ACS Nano*, 2025, **19**, 281–306.

21 W. He, R. T. K. Kwok, Z. Qiu, Z. Zhao and B. Z. Tang, A Holistic Perspective on Living Aggregate, *J. Am. Chem. Soc.*, 2024, **146**, 5030–5044.

22 H. Wang, E. Zhao, J. W. Y. Lam and B. Z. Tang, AIE luminogens: emission brightened by aggregation, *Mater. Today*, 2015, **18**, 365–377.

23 R. Hu, N. L. C. Leung and B. Z. Tang, AIE macromolecules: syntheses, structures and functionalities, *Chem. Soc. Rev.*, 2014, **43**, 4494–4562.
24 N. K. S. Teo, B. Fan, A. Ardana and S. H. Thang, Aggregation-induced emission polymers via reversible-deactivation radical polymerization, *Aggregate*, 2024, **5**, e414.
25 Y. Sun, K. Wang, X. Huang, S. Wei, E. Contreras, P. K. Jain, L. M. Campos, H. J. Kulik and J. S. Moore, Caged AIEgens: Multicolor and White Emission Triggered by Mechanical Activation, *J. Am. Chem. Soc.*, 2024, **146**, 27117–27126.
26 C. Ma, T. Han, N. Niu, L. Al-Shok, S. Efstathiou, D. Lester, S. Huband and D. Haddleton, Well-defined polyacrylamides with AIE properties via rapid Cu-mediated living radical polymerization in aqueous solution: thermoresponsive nanoparticles for bioimaging, *Polym. Chem.*, 2022, **13**, 58–68.
27 C. Zhang, X. Yao, J. Wang and X. Ma, Tunable emission of a tetraphenylethylene copolymer via polymer matrix assisted and aggregation-induced emission, *Polym. Chem.*, 2017, **8**, 4835–4841.
28 R. A. Shilov, V. A. Baigildin, K. S. Kisel, E. E. Galenko, A. S. Gubarev, M. E. Mikhailova, O. S. Vezo, N. V. Tsvetkov, A. A. Shtyrov, M. N. Ryazantsev, J. R. Shakirova and S. P. Tunik, RAFT Copolymerization of Pt(II) Pincer Complexes With Water-Soluble Polymer as an Efficient Way to Obtain Micellar-Type Nanoparticles With Aggregation-Induced NIR Emission, *Aggregate*, 2024, e713.
29 E. R. Sauvé, C. M. Tonge and Z. M. Hudson, Aggregation-Induced Energy Transfer in Color-Tunable Multiblock Bottlebrush Nanofibers, *J. Am. Chem. Soc.*, 2019, **141**, 16422–16431.
30 K. Kokado, R. Taniguchi and K. Sada, Rigidity-induced emission enhancement of network polymers crosslinked by tetraphenylethene derivatives, *J. Mater. Chem. C*, 2015, **3**, 8504–8509.
31 J. Poisson, C. M. Tonge, N. R. Paisley, E. R. Sauvé, H. McMillan, S. V. Halldorson and Z. M. Hudson, Exploring the Scope of Through-Space Charge-Transfer Thermally Activated Delayed Fluorescence in Acrylic Donor–Acceptor Copolymers, *Macromolecules*, 2021, **54**, 2466–2476.
32 S. Ye, N. Meftahi, I. Lyskov, T. Tian, R. Whitfield, S. Kumar, A. J. Christofferson, D. A. Winkler, C.-J. Shih, S. Russo, J.-C. Leroux and Y. Bao, Machine learning-assisted exploration of a versatile polymer platform with charge transfer-dependent full-color emission, *Chem*, 2023, **9**, 924–947.
33 S. Ye, T. Tian, A. J. Christofferson, S. Erikson, J. Jagielski, Z. Luo, S. Kumar, C.-J. Shih, J.-C. Leroux and Y. Bao, Continuous color tuning of single-fluorophore emission via polymerization-mediated through-space charge transfer, *Sci. Adv.*, 2021, **7**, eabd1794.
34 C. M. Tonge and Z. M. Hudson, Interface-Dependent Aggregation-Induced Delayed Fluorescence in Bottlebrush Polymer Nanofibers, *J. Am. Chem. Soc.*, 2019, **141**, 13970–13976.
35 K. Nakabayashi, M. Takata, M. Furukawa and H. Mori, Luminescent core–shell nanoparticles with crosslinked aggregation-induced emission core structures: Emission both in solution and solid states, *J. Polym. Sci.*, 2020, **58**, 852–859.
36 M. A. López-Quintela, C. Tojo, M. C. Blanco, L. García Rio and J. R. Leis, Microemulsion dynamics and reactions in microemulsions, *Curr. Opin. Colloid Interface Sci.*, 2004, **9**, 264–278.
37 Y. Wang, Z. Liu, A. Mazumder, C. G. Gianopoulos, K. Kirschbaum, L. A. Peteanu and R. Jin, Tailoring Carbon Tails of Ligands on Au52(SR)32 Nanoclusters Enhances the Near-Infrared Photoluminescence Quantum Yield from 3.8 to 18.3%, *J. Am. Chem. Soc.*, 2023, **145**, 26328–26338.
38 P. Chaibuth, N. Chuaytanee, J. Hojitsiriyanont, K. Chainok, S. Wacharasindhu, O. Reiser and M. Sukwattanasinitt, Copper(ii) complexes of quinoline-based ligands for efficient photoredox catalysis of atom transfer radical addition (ATRA) reaction, *New J. Chem.*, 2022, **46**, 12158–12168.
39 S. Feng, L. Zhu, D. Wang, C. Li, Y. Chen, X. Chen, J. Liu, W. Huang, Y. Ling and W. Huang, Rigidity-Tuned Full-Color Emission: Uncommon Luminescence Change from Polymer Free-Volume Variations, *Adv. Mater.*, 2022, **34**, 2201337.
40 W. Jakubowski, B. Kirci-Denizli, R. R. Gil and K. Matyjaszewski, Polystyrene with Improved Chain-End Functionality and Higher Molecular Weight by ARGET ATRP, *Macromol. Chem. Phys.*, 2008, **209**, 32–39.
41 G. Gazzola, I. Filipucci, A. Rossa, K. Matyjaszewski, F. Lorandi and E. M. Benetti, Oxygen Tolerance during Surface-Initiated Photo-ATRP: Tips and Tricks for Making Brushes under Environmental Conditions, *ACS Macro Lett.*, 2023, **12**, 1166–1172.
42 G. Szczepaniak, J. Jeong, K. Kapil, S. Dadashi-Silab, S. S. Yerneni, P. Ratajczyk, S. Lathwal, D. J. Schild, S. R. Das and K. Matyjaszewski, Open-air green-light-driven ATRP enabled by dual photoredox/copper catalysis, *Chem. Sci.*, 2022, **13**, 11540–11550.
43 J. Wang, H. Huang and X. Huang, Molecular weight and the Mark-Houwink relation for ultra-high molecular weight charged polyacrylamide determined using automatic batch mode multi-angle light scattering, *J. Appl. Polym. Sci.*, 2016, **133**, 43748.
44 L. Michalek, L. Barner and C. Barner-Kowollik, Polymer on Top: Current Limits and Future Perspectives of Quantitatively Evaluating Surface Grafting, *Adv. Mater.*, 2018, **30**, 1706321.
45 Z. Wang, J. Lee, Z. Wang, Y. Zhao, J. Yan, Y. Lin, S. Li, T. Liu, M. Olszewski, J. Pietrasik, M. R. Bockstaller and K. Matyjaszewski, Tunable Assembly of Block Copolymer Tethered Particle Brushes by Surface-Initiated Atom Transfer Radical Polymerization, *ACS Macro Lett.*, 2020, **9**, 806–812.